Marine and Petroleum Geology 103 (2019) 473–484

Contents lists available at ScienceDirect

Marine and Petroleum Geology

journal homepage: www.elsevier.com/locate/marpetgeo

Research paper

Multi-proxy analysis of organic matter accumulation in the Upper Ordovician–Lower Silurian black shale on the Upper Yangtze Platform, south China

Xiaoqi Wang[a,b], Yanming Zhu[a,b,*], Gary G. Lash[c], Yang Wang[a,b]

[a] Key Laboratory of Coal Bed Methane Resource & Reservoir Formation Process of the Ministry of Education, China University of Mining & Technology, Xuzhou, 221116, China
[b] School of Resources and Earth Science, China University of Mining & Technology, Xuzhou, 221116, China
[c] Department of Geology and Environmental Science, State University of New York at Fredonia, Fredonia, NY, 14063, USA

ARTICLE INFO

Keywords:
Organic-rich shale
Palaeoenvironment
Trace elements
Redox conditions
Paleoproductivity
Organic matter accumulation

ABSTRACT

There is no doubt that organic matter plays an important role in shale gas accumulation and storage. Thus, successful evaluation and production strategies of organic-rich shale deposits require an understanding of the range of factors that contribute to the accumulation and preservation of organic matter in these deposits. This paper reports results of a multi-faceted study of two Ordovician–Silurian transition sections of the Upper Yangtze Platform of South China. Organic and inorganic geochemical data are used to reconstruct paleoenvironmental changes across this critical interval of Earth history and to identify those factors that were most important to organic matter accumulation. Deposition of organic-rich shale of the Katian lower Wufeng Formation was favored by rising sea level and diminished clastic sediment content. Black shale of the upper Wufeng preceded Hirnantian glaciation whereas the overlying lower Longmaxi Formation accumulated in association with a post-glacial rise of sea level as well as the peak of Caledonian tectonism. The carbonaceous deposits appear to reflect the combined effects of elevated primary productivity as suggested by Si/Al and Ti/Al ratios, especially in the upper Wufeng, and consequent depletion of water column oxygen (preservation). Consideration of the relationships of redox-sensitive trace element concentrations and total organic carbon content suggest that bottom water conditions fluctuated between anoxic and euxinic during this period, perhaps related to rapid oscillations of sea level. Moreover, the basin appears to have remained connected with the global ocean in spite of Caledonian uplift of bordering areas. Thus, black shale sedimentation on the Upper Yangtze Platform at the Ordovician-Silurian boundary reflects the interplay of climate change and tectonism and their influences on sea level, clastic sediment content, and paleo-productivity.

1. Introduction

Upper Ordovician–Lower Silurian black shale of the Wufeng and Longmaxi formations of South China, regarded as a high quality hydrocarbon source rock, has been the focus of recent exploration and production efforts (Tan et al., 2014; Dong et al., 2015). Indeed, a considerable body of literature detailing shale reservoir characteristics and shale gas accumulation processes exists for these deposits. Many of these studies demonstrate the significant role that organic matter plays in controlling a range of shale reservoir properties, including the volume of nano-scale porosity that serves as gas storage space (Curtis, 2002; Jarvie et al., 2007; Chen and Xiao, 2014; Yu et al., 2016; He et al., 2017; Yang et al., 2017). Additionally, organic carbon content is critical to gas adsorption capacity and potential seepage of the host shale (Li et al., 2008; Clarkson et al., 2013; Zhang et al., 2015; Yang et al., 2016a,b; Wang et al., 2016; X. Wang et al., 2019). Thus, acquiring a robust understanding of the enrichment mechanisms of organic matter in black shale provides a sound geological basis for exploration and development strategies of shale gas.

The most commonly cited controls of organic enrichment of fine-grained source rocks include biological productivity or organic carbon flux, bottom water oxygen concentration, and sediment accumulation rates (Demaison and Moore, 1980; Ibach, 1980; Pedersen, 1990; Calvert et al., 1992; Sageman et al., 2003; Bohacs et al., 2005). Less than 10%

* Corresponding author. Key Laboratory of Coal Bed Methane Resource & Reservoir Formation Process of the Ministry of Education, China University of Mining & Technology, Xuzhou, 221116, China.
E-mail address: ymzhucumt@126.com (Y. Zhu).

https://doi.org/10.1016/j.marpetgeo.2019.03.013
Received 25 September 2018; Received in revised form 6 March 2019; Accepted 11 March 2019
Available online 14 March 2019
0264-8172/

of organic matter produced in the euphotic zone survives transport through the water column to accumulate on the sea floor (Passey et al., 2010). Further, much of the deposited organic matter is quickly consumed by metazoan and micro organisms at the sediment-water interface or a short distance into the sediment column. Ultimately, perhaps only 0.1–1.0% of organic matter produced at the ocean surface remains after burial (Vandenbroucke and Largeau, 2007). The described scenario is negatively impacted by the dilutive effects of high sedimentation rates (Passey et al., 2010) though very low rates tend to favor the oxidative loss of organic matter settling through the water column (Ibach, 1980).

It is apparent that the evaluation of source rock quality is strengthened by a sound understanding of the depositional and post-depositional conditions of the organic-rich deposit. Indeed, varying elemental abundances through a stratigraphic succession reflect evolving physicochemical conditions, bottom water and diagenetic, in that region of the basin (Murray, 1994; Lev et al., 1998; Tribovillard et al., 2006; Franchi et al., 2016). Trace and rare earth element (REE) geochemistry has been shown to be especially valuable to the evaluation of the range of factors that controls the production, accumulation, and preservation of organic matter, including paleoclimate, bioproductivity, redox conditions, sedimentation rate, and sea level change (Barberi and Leoni, 2003; Sageman et al., 2003; Werne et al., 2003; Algeo and Maynard, 2004; Rimmer, 2004; Rimmer et al., 2004; Algeo and Lyons, 2006; Tribovillard et al., 2006; Calvert and Pedersen, 2007; Lash and Blood, 2014).

Redox-sensitive trace elements (RSTEs), including U, V and Mo, are considered especially useful to paleoenvironmental reconstruction of sediment that accumulated underoxygen-deficient and/or sulfidic bottom-water conditions (Algeo and Maynard, 2004; Algeo and Lyons, 2006; Tribovillard et al., 2009; Scott and Lyons, 2012; Algeo and Rowe, 2012). Phosphorus and barium are known to display strong positive covariance with other productivity indicators in modern marine deposits demonstrating their potential as a proxies of primary surface productivity in ancient deposits (Bishop, 1988; Schmitz, 1987; Dymond et al., 1992; Paytan et al., 1996; Sanchez-Vidal et al., 2005). It is important to bear in mind, however, that evaluation of paleoproductivity by correlation of elemental proxies with organic carbon content may be hindered by organic losses within the water column and sediment (Schoepfer et al., 2015).

Recent research efforts have focused on the mineralogy and geochemistry, rock fabric, biological composition, and stratigraphic framework of the Wufeng and Longmaxi formations of the Upper Yangtze Platform (Liu et al., 2017; Wang et al., 2018, 2019; C. Wang et al., 2018; Yan et al., 2018; Zhang et al., 2018; Y. Wang et al., 2019). Though they have contributed much to our understanding of the factors that influenced deposition of the Wufeng and Longmaxi, there is much to be considered regarding paleoproductivity by use of the more recently described proxies (Schoepfer et al., 2015). Moreover, the more conventional view of a restricted basin during the Ordovician-Silurian transition may not be valid. This paper considers major and trace element concentrations spanning the Wufeng Formation and overlying Longmaxi Formation of the Upper Yangtze Platform, southeast of Chongqing City, South China, in order to elucidate paleoenvironmental conditions associated with their accumulation at the Ordovician-Silurian transition, an especially critical interval of Earth history. Our study provides the basis for broader assessment of Late Ordovician and Early Silurian organic matter accumulation patterns of the expansive Upper Yangtze region. Finally, results of the present study will contribute to shale gas-in-place estimation and reservoir evaluation of the marine shale succession of the Upper Yangtze Platform.

1.1. Geological setting

The Yangtze Platform lay close to the paleo-equator during Late Ordovician time (Fig. 1) (Metcalfe, 1994; Zhou et al., 2015). An episode of rising sea level coincident with the *Dicellograptus complexus* (*D.com.*) Zone of the middle Katian Stage was accompanied by deposition of siliceous organic-rich shale of the Wufeng Formation (Fig. 2) (Chen et al., 1987). A subsequent eustatic fall associated with Hirnantian glaciation resulted in widespread deposition of calcareous mudstone and limestone of the Kuanyinchiao Bed characterized by a low diversity graptolite fauna corresponding with the *Normalograptus extraordinarius*-N.*ojsuensis* Zone (Fig. 2) (Chen, 1984; Brenchley et al., 1994, 2003; Xu et al., 2000, 2004; Chen et al., 2006). The peak of Caledonian tectonism during the late Hirnantian – early Rhuddanian interval resulted in uplift on the west, south, and east of the Yangtze Platform, including the Dianqian and Chendu uplifts (Fig. 3), thus forming a semi-enclosed basin (Wang et al., 1997; Xu et al., 2004; Liang et al., 2009). A contemporaneous global sea level rise was accompanied by widespread accumulation of black shale deposits of the lower Longmaxi Formation spanning the *Normalograptus persculptus* (*N.per*), *Akidograptus ascensus* (*A.asc.*), and *Parakidograptus acuminatus* Zones (*P.acu.*) (Fig. 2) (Chen, 1984; Xu et al., 2000, 2004).

2. Samples and analysis

2.1. Samples

Forty black shale samples were collected from the Pengshui (PG) and Youyang (YY) sections (Fig. 3). Both newly excavated sections preserve an essentially complete Upper Ordovician to Lower Silurian succession. The PG section (29°08′42″N, 108°17′36.6″E) is located about 160 km southeast of Chongqing City and the YY section (29°04′31″N,108°16′57.7″E) is approximately 50 km southeast of the PG section (Fig. 3). Twenty samples were recovered from each section, including 7 from the Wufeng Formation and 13 from the Longmaxi Formation.

2.2. Analytical procedures

Approximately 3 g of each sample was crushed to gravel-size particles, powdered to finer than 200 mesh size using an agate mortar, and split into three equal parts. Powdered sample splits analyzed for total organic carbon (TOC) were treated with 10% hydrochloric acid (HCl) to remove carbonate. The remaining HCl was removed with distilled water and the residue was analyzed using a LECO CS-344 carbon-sulfur analyzer at the Key Laboratory of Coalbed Methane Resources and Reservoir Formation Process of the Ministry of Education (CUMT). Instrument accuracy is ± 0.5%.

Approximately 1 g of each sample split used for major element analysis (Si, Al, Ca, Fe, K, Mg, Ti, and P) was burned in a muffle furnace at 900 °C for 3–4 h to remove organic matter and carbonate. Each cooled ashed sample was weighed and the mass lost on combustion was recorded for correction. Finally, about half of the powder was mixed with 8 times lithium tetraborate ($Li_2B_4O_7$), fused into glass beads, and analyzed on a Rigaku 100eX-ray fluorescence (XRF) spectrometer. The measurement error ranges from 1 to 5%.

Sample splits for trace element analysis were dissolved in a PicoTrace High Pressure Dissolution System. Initially, 100–120 mg of powder was weighed and diluted with 1 ml of deionized water to prevent the reactor from drying. Following this, 3 mL of high-concentration HF was added to each sample, which was allowed to stand 24 h to remove siliceous material. Samples were then treated with 3 mL HNO_3, 3 ml HF, and 1.5 ml $HClO_4$ in a Teflon bomb and heated to 180 °C for 20 h. When they had dried, another 80 ml HNO_3 was added to each sample after which they were heated. Finally, the residue was redissolved in 15 ml HNO_3 and $HClO_4$. Each sample solution was diluted to 3% HNO_3 with a factor of 1/2000 for ICP-MS analysis. Analytical precision wasgenerally less than 5%.

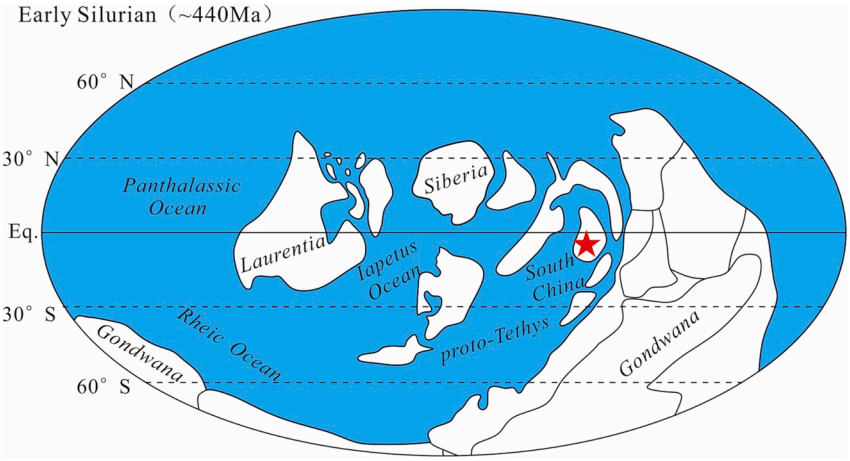

Fig. 1. Global paleogeographic map (~453–445 Ma) showing the location of South China (Zhou et al., 2015). The red star represents the study location area.

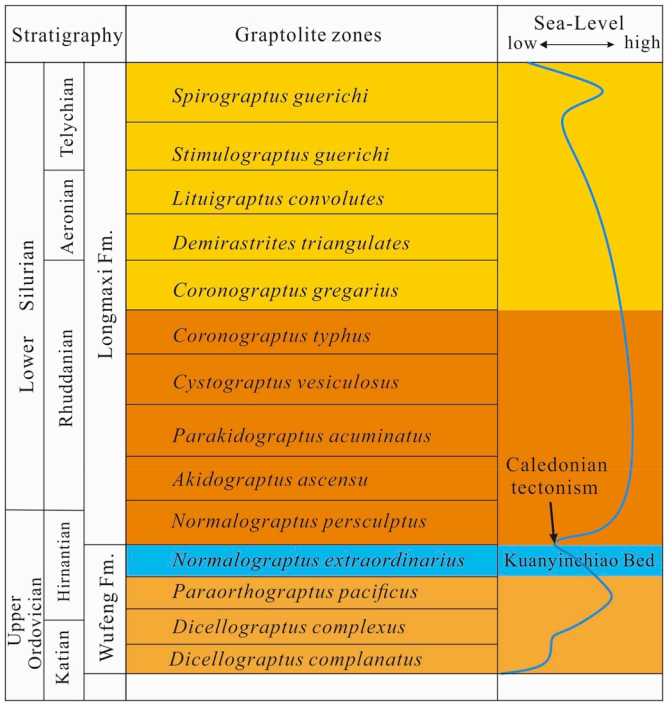

Fig. 2. Graptolite biostratigraphy (Xu et al., 2000) and sea level history (Haq and Schutter, 2008) through the Ordovician and Silurian transition.

2.3. Data presentation

Trace element compositions of sediment generally include various proportions of terrestrial/clastic and authigenic components (Calvert and Pedersen, 2007). The latter reflects water column geochemistry and redox conditions of the depositional and pore-water environment (Jiang et al., 2007). Aluminum is considered to be the principal conservative or stable proxy for clay mineral content in fine-grained clastic deposits (Arthur, 1985; Arthur and Dean, 1991; Calvert and Pedersen, 2007). Aluminum normalization is commonly employed as a means of comparing the normalized measured concentration of a specific element with that ratio documented for a composite of shales, including the Post Archean Australian Shale (PAAS; McLennan, 2001). The normalization process is improved by calculation of enrichment factors (Tribovillard et al., 2006; Li et al., 2017) as the following equation:

$$(\text{X-EF}) = (\text{X/Al})_{\text{sample}}/(\text{X/Al})_{\text{PAAS}} \quad (1)$$

in which X - EF is the enrichment factor of element X, $(X/Al)_{sample}$ is the ratio of element X to Al measured in the sample, and $(X/Al)_{PAAS}$ is the ratio of PAAS values of element X to Al. X-EF > 3 is interpreted to reflect a detectable enrichment relative to the standard (Tribovillard et al., 2012) whereas X-EF < 1 specifies a depleted concentration. REE data are normalized to chondrite values (Haskin et al., 1966) and the North American Shale Composite (NASC; Gromet et al., 1984).

The abundance of organically sourced P (P_{org}) is calculated by the following equation:

$$P_{org} = P_{sample}\text{-}Al_{sample} \times (P/Al)_{PAAS} \quad (2)$$

where P_{sample} and Al_{sample} areP and Al concentrations of the sample, respectively, and $(P/Al)_{PAAS}$ is the P/Al of Post Archean Australian Shale. Similarly, the concentration of Ba derived from biogenic sources (Ba_{bio})was calculated using the following equation:

$$Ba_{bio} = Ba_{sample}\text{-}Al_{sample} \times (Ba/Al)_{PAAS}. \quad (3)$$

Mass accumulation rates (MAR) were calculated using productivity of the present study (TOC, P_{org}, and Ba_{bio})as deescribed by Schoepfer et al. (2015). MAR values of the various productivity proxies (XMAR) were calculated according to the following expression:

$$XMAR = [X] \times XBAR \quad (4)$$

where [X] refers to the concentration of TOC, P_{org}, or Ba_{bio}. The bulk accumulation rate of proxy X (XBAR) is calculated as follows:

$$XBAR = \rho \times LSR \quad (5)$$

where ρ is the bulk density of shale (g cm^{-3}) and LSR is the calculated linear sedimentation rate (cm kyr^{-1}) The data of these two variables are Based on previous data (Deng et al., 2018; Y. Wang et al., 2018).

3. Results

3.1. Total organic carbon (TOC) content

The TOC content of the PG section ranges from 1.1 to 10.5% (average = 3.8%) and 0.2–7.9% (average = 3.6%) in the YY section (Figs. 4 and 5). TOC is greatest (> 2%) in the lower Wufeng and Longmaxi formations (Figs. 4 and 5). It is noteworthy that TOC of the most carbonaceous interval of the YY section is markedly less than that of the PG section (Figs. 4 and 5).

3.2. Major elements

The dominant oxides of the studied samples include, in descending order of abundance, SiO_2, Al_2O_3 and CaO. Among these, SiO_2 displays

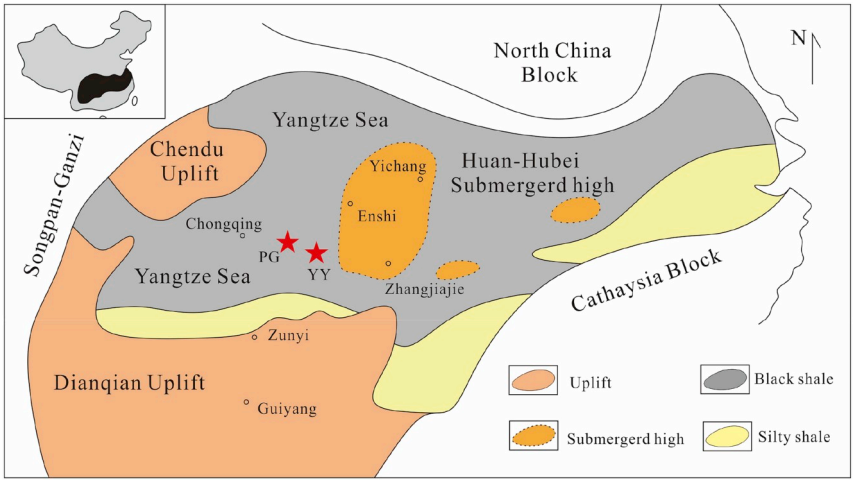

Fig. 3. Paleogeographic map of the Yangtze Platform during Late Ordovician to Early Silurian (modified from Chen et al. and Zhou et al., 2015). Study sections (indicated by the red stars): PG: Pengshui, Chongqing; YY: Youyang, Chongqing.

the greatest concentration, ranging from 10.0 to 88.6% (average = 61.6%) (Figs. 4 and 5). CaO of the studied sections ranges from 0.2 to 47.3% (average = 10.7%) (Figs. 4 and 5) and Al_2O_3 varies from 2.2 to 17.7% (average = 9.7%) (Figs. 4 and 5). Overall, the Wufeng and lower Longmaxi formations display the greatest concentrations of SiO_2 and CaO though SiO_2 values are invariant through much of the Longmaxi Formation of both sections (Figs. 4 and 5).

3.3. Trace elements

Degrees of enrichment of RSTEs Mo, V, and U co-vary positively with each other in both sections ($r > 0.71$, $p(\alpha) < 0.01$, $n = 20$; Fig. 6). The lower half of the Wufeng Formation, especially in the PG section, displays generally low or irregular enrichment values of these elements (Figs. 7 and 8). Elevated enrichment higher in the Wufeng continues into the lower Longmaxi Formation of both sections (Figs. 7 and 8). Redox-sensitive element enrichment diminishes upward through the Longmaxi though it appears to increase at the top of the YY section (Figs. 7 and 8).

Cu and Ni display increasing enrichment upward through the Wufeng Formation into the lower Longmaxi Formation (Figs. 7 and 8). With the exception of the basal Wufeng Formation, vertical trends of Cu and especially Ni enrichment mimic the TOC profiles (Figs. 7 and 8). The enrichment trend of Ba in the PG section generally follows that of Ni and, to a lesser extent, Cu (Fig. 7). Indeed, co-variance of Cu and Ni ($r = +0.71$, $p(\alpha) < 0.01$, $n = 20$)in the PG section is stronger than that of Ba and Ni ($r = +0.49$, $0.01 < p(\alpha) < 0.05$, $n = 20$) and Ba and Cu ($r = +0.52$, $0.01 < p(\alpha) < 0.05$, $n = 20$) (Fig. 6). However, co-variance of Cu and Ni ($r = +0.65$, $p(\alpha) < 0.01$, $n = 20$) is little changed in the YY section from that of the PG section, yet Ba and Cu ($r = 0.38$, $p(\alpha) > 0.05$, $n = 20$) display markedly diminished co-variance (Fig. 6). The generally low co-variance of TOC with Cu, Ni, and Ba in both sections (Fig. 6) suggests that measured TOC values of the Wufeng and Longmaxi formations have been modified by hydrocarbon generation.

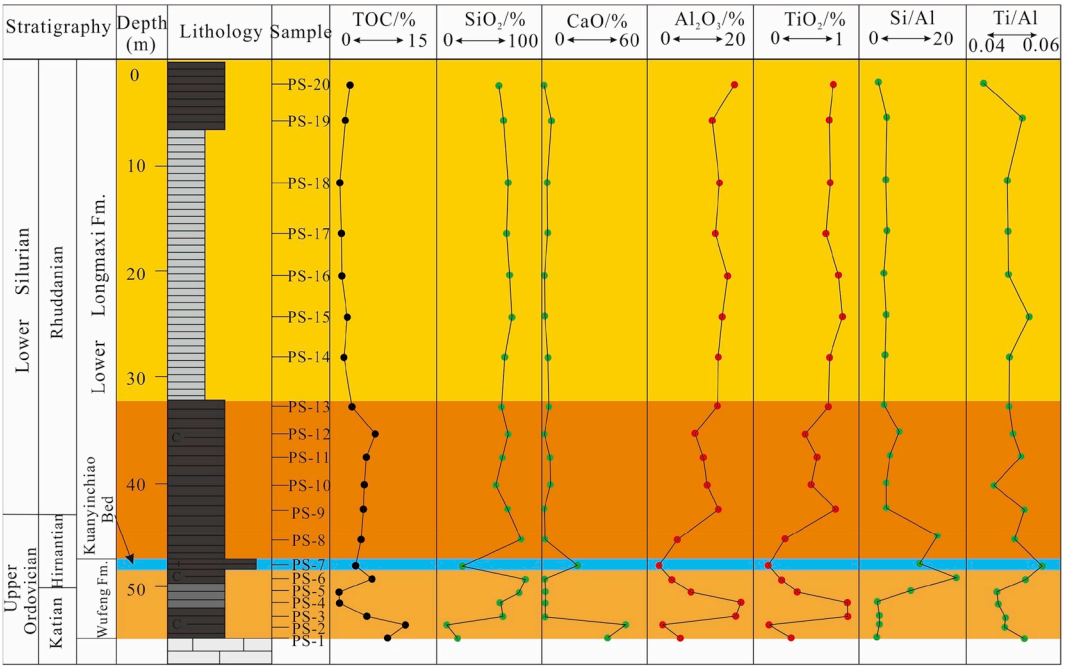

Fig. 4. Geochemical profiles of the PG section displaying TOC (%), SiO_2(%), CaO (%), Al_2O_3(%), TiO_2(%), Si/Al, and Ti/Al. Sample locations are found to the left of the TOC profile.

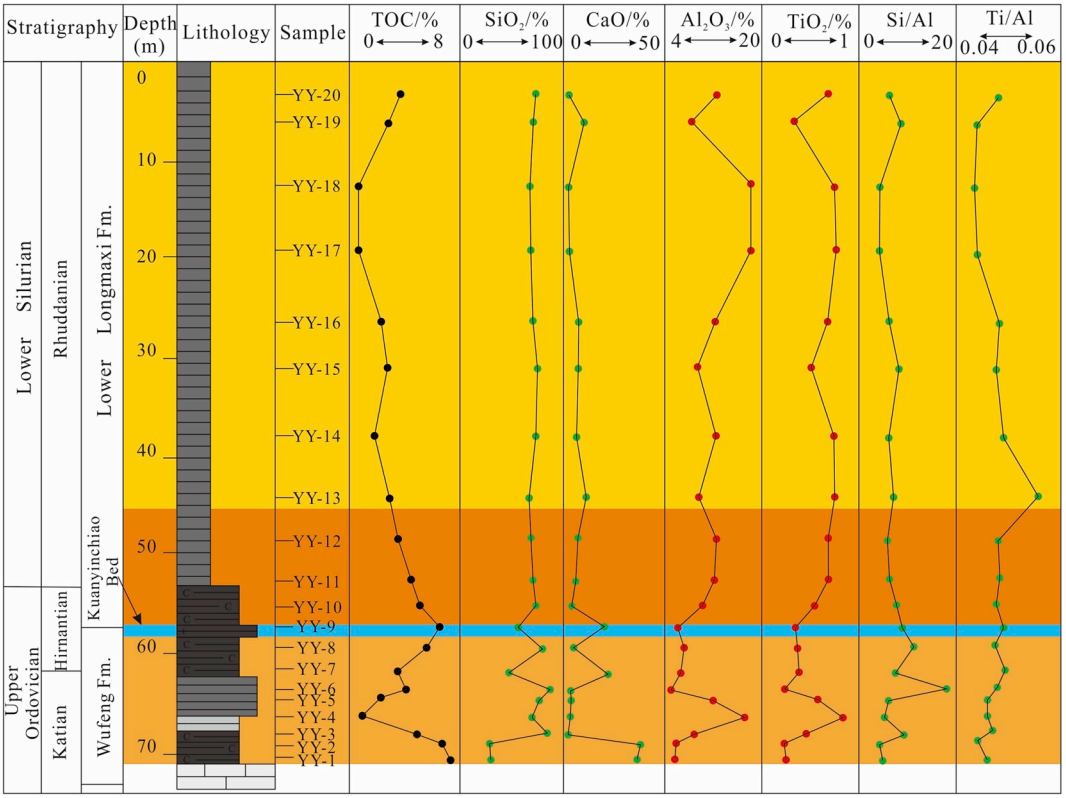

Fig. 5. Geochemical profiles of theYY section displaying TOC (%), SiO_2(%), CaO (%), Al_2O_3(%), TiO_2(%), Si/Al, and Ti/Al. Sample locations are found to the left of the TOC profile.

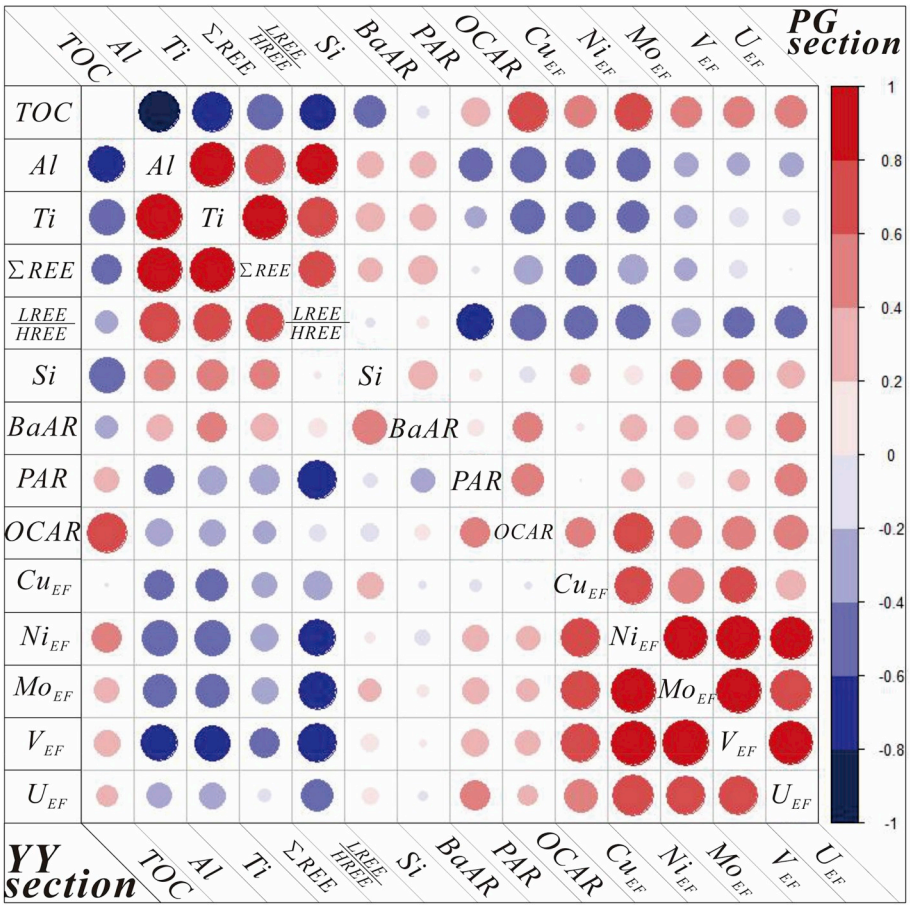

Fig. 6. Correlation coefficients of organic and inorganic geochemical data for the PG (Upper right triangle)and YY sections (Lower left triangle).The correlation coefficient is represented by a filled circle of gradient colors (red for the correlation coefficient and blue for the negative number). The greater the absolute value of the correlation coefficient, the greater the radius of the corresponding circle. Correlation coefficient values are shown in Table 1. (For interpretation of the references to color in this figure legend, the reader is referred to the Web version of this article.)

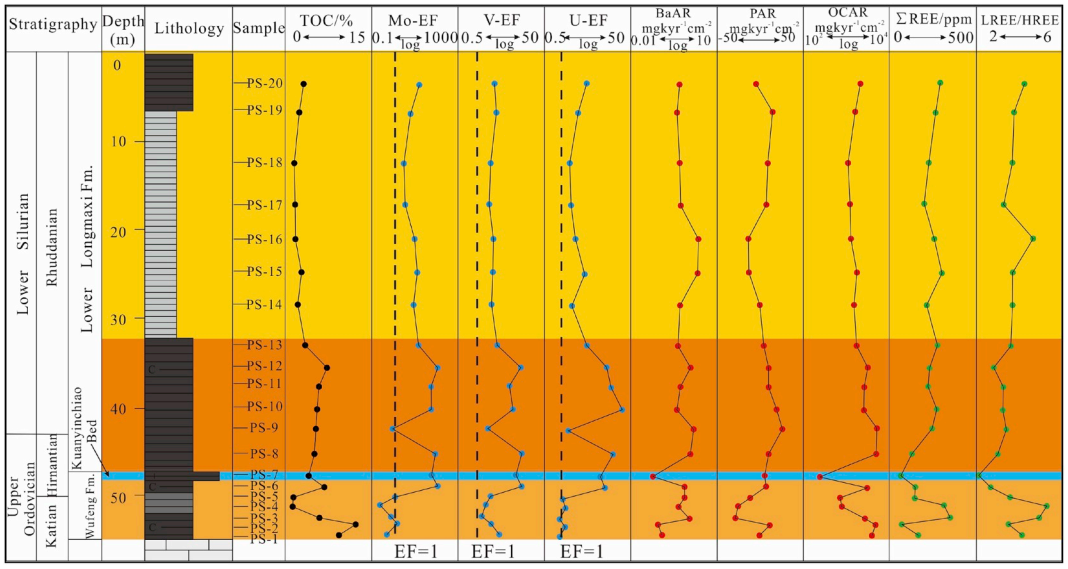

Fig. 7. Geochemical profiles of the PG section displaying TOC (%), Mo EF, V EF, U EF, BaAR, PAR, OCAR, ΣLREE (ppm) and LREE/HREE. Sample locations are foundto the left of the TOC profile.

3.4. Rare earth elements

Chondrite-normalized REE concentrations display relative enrichment of light REEs (LREEs) and, in most samples, a negative Eu anomaly (Fig. 9A and B). NASC-normalized REE concentration patterns are generally flatter than chondrite-normalized patterns indicating generally consistent concentrations of light and heavy REEs of the studied samples and the NASC standard (Fig. 9C and D). However, samples from the top of Wufeng Formation and the bottom of Longmaxi Formation display negative Ce anomalies (Fig. 9C and D).

The ratio of total light to total REEs (ΣLREE/ΣHREE) ranges from 2.1 to 5.3 (average = 3.6) for the PG section and 2.6 to 4.4 (average = 3.3)for the YY section (Figs. 7 and 8). In general, the Wufeng Formation of both locations displays diminishing ΣLREE/ΣHREE up-section (Figs. 7 and 8). The overlying Longmaxi Formation of both sections is characterized by increasing ΣLREE/ΣHREE (Figs. 7 and 8). It is noteworthy that the lower Wufeng Formation of the PG section displays the highest ΣLREE/ΣHREE values of both sections (Figs. 7 and 8). The relatively strong positive co-variance of ΣLREE/ΣHREE and ΣREE of both sections ($r = +0.66$, $0.01 < p(\alpha) < 0.05$, $n = 20$, PG section; $r = +0.63$, $0.01 < p(\alpha) < 0.05$, $n = 20$, YY section) reflects enrichment of LREE (Figs. 7 and 8). Finally, ΣREE and Al_2O_3 and TiO_2 of both sections display very strong positive co-variance (Figs. 4–6).

ΣREE displays variable degrees of co-variance with major and trace elements (Fig. 6). The strongest positive correlations are those with Al_2O_3 and TiO_2, especially in the PG section (Fig. 6). It is noteworthy that ΣREE displays low negative correlations with RSTEs (Fig. 6).

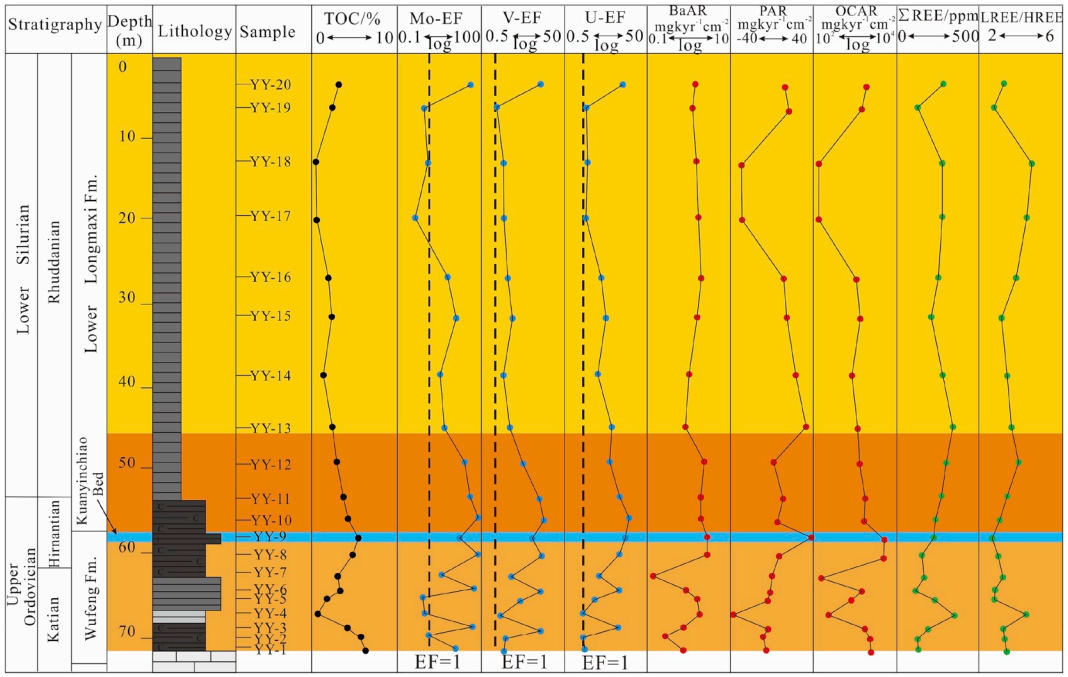

Fig. 8. Geochemical profiles of the YY section displaying TOC (%), Mo EF, V EF, U EF, BaAR, PAR, OCAR, ΣLREE (ppm) and LREE/HREE. Sample locations are found to the left of the TOC profile.

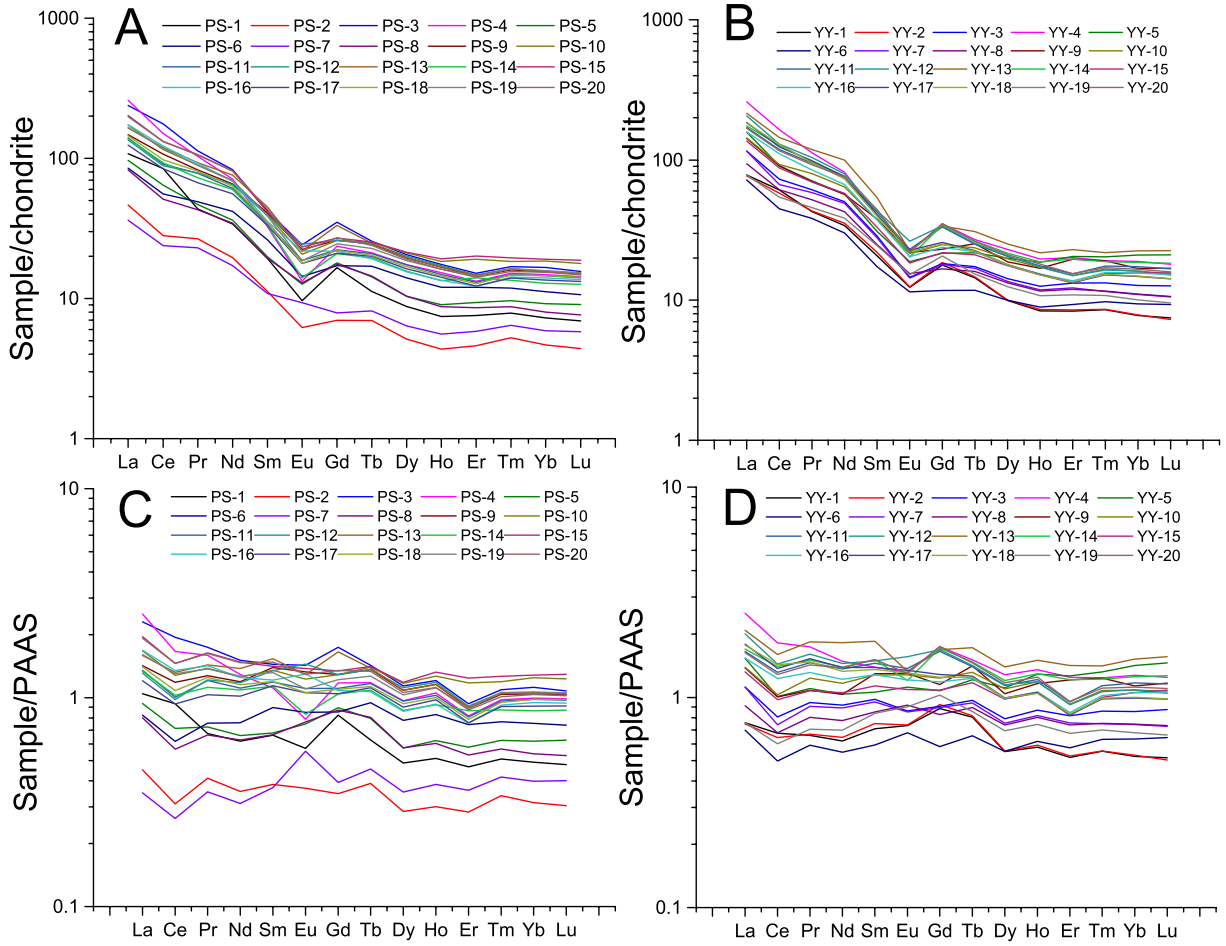

Fig. 9. REE concentrations normalized to chondrite of the (A)PG section; and (B) YY section; REE concentrationsnormalized to NASC of the (C) PG section; and (D)YY section.

4. Discussion

4.1. Terrigenous content

Aluminum and Ti are incompatible elements that have relatively short residence times in seawater and very stable chemical properties. These elements are generally interpreted to reflect the lithogenous fractionof a sediment (Norman and Deckker, 1990; Calvert and Pedersen, 2007). Low concentrations of Al and Ti in the lower and upper third of the Wufeng Formation (Figs. 4 and 5) suggest a muted content of clastic sediment during these time intervals. The thin interval of elevated Al and Ti in the middle of the Wufeng (Figs. 4 and 5) likely reflects a pulse of clastic sediment delivery during a protracted period of otherwise diminished clastic content. Increasing Al and Ti at the Wufeng-Longmaxi contact continues more subtly upward through both sections, a likely reflection of an increased content of clastic sediment contemporaneous with deposition of this unit. Moreover, the strong covariance of ΣREE and Al_2O_3 and TiO_2 of both sections (Figs. 4 and 5) suggests that REEs were sourced principally from the lithogenous fraction.

Grain size variations of the detrital fraction are reflected by abundance fluctuations of those elements typically associated with the coarser sediment fraction relative to Al, including Ti and Si (Sageman and Lyons, 2004; VerStraeten et al., 2011). Aluminum-normalized Si reflects the ratio of quartz to aluminosilicate phases in sediment thus providing a qualitative measure of coarse-versus fine-grained sediment (VerStraeten et al., 2011). However, caution must be exercised when interpreting Si/Al ratios as Si contained within opaline skeletal remains of diatoms, silicoflagellates, and radiolarians accumulates independent of clay content (Calvert and Pedersen, 2007). Indeed, petrographic analysis of Wufeng and Longmaxi samples reveals the presence of sponge spicules and radiolarian tests (Fig. 10). The generally conservative element Ti is thought to be contributed chiefly by high density minerals, notably rutile, sphene, and ilmenite (Schütz and Rahn, 1982; Dypvik and Harris, 2001; Calvert and Pedersen, 2007) making Ti/Al a useful proxy for grain size (Boyle, 1983; Shimmield and Mowbray, 1991; Schneider et al., 1997; Zabel et al., 1999, 2001). Si/Al values of both sections define a baseline value of ~5, which exceeds the average shale value of 3.11 (Wedepohl, 1971, 1991) and reflects the siliceous nature of these deposits. Increases of Si/Al, especially obvious in the PG section, are found from the middle of the Wufeng Formation near the Katian-Hirnantian boundary extending into the lower Longmaxi Formation to approximately the Hirnantian-Rhuddanian boundary (Figs. 4 and 5). Both Si/Al excursions correspond with intervals of diminished Al_2O_3 in the upper half of the Wufeng Formation. The fact that the above-mentioned Si/Al excursions do not correspond with similar deviations of Ti/Al (Figs. 4 and 5) suggests that elevated Si was partly the result of an elevated content of biogenic silica associated with increased productivity.

4.2. Paleoredox conditions

The low solubility of RSTEs under oxygen-depleted conditions favors the enrichment of sediment deposited under oxygen-depleted conditions in these elements (Algeo and Maynard, 2004; Algeo and Lyons, 2006; Tribovillard et al., 2006; Algeo and Tribovillard, 2009;

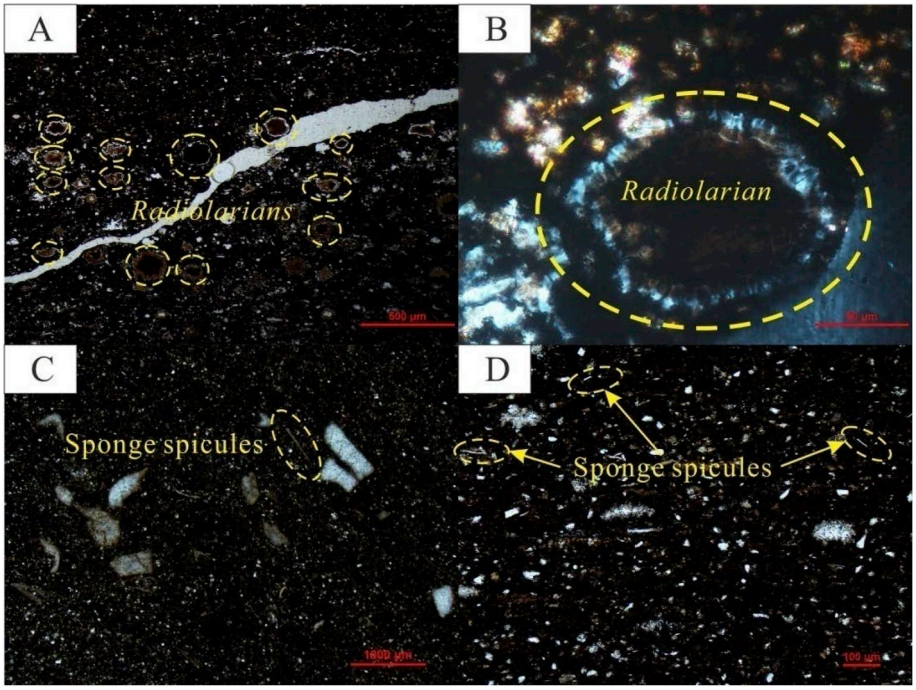

Fig. 10. Photomicrographs of studied samples displaying (A,B) radioaria (sample YY-2)and (C, D) sponge spicules (sample PS-7).

Algeo and Rowe, 2012).Trends of redox-sensitive proxies suggest that the studied Ordovician-Silurian transition interval preserves the record of rapidly fluctuating redox conditions. Mo, U, and V EF values < 3 in the lower Wufeng Formation, especially the PG section (Figs. 7 and 8), reflect sedimentation under oxygenated bottom conditions (Liu et al., 2017; Yan et al., 2018). The upper Wufeng and lower Longmaxi formations display marked enrichments of Mo, U, and V suggesting the establishment of anoxic, perhaps euxinic, bottom-water conditions (Yan et al., 2015, 2018; Ma et al., 2016; Huang et al., 2017; Liu et al., 2017). A generally gradual reduction of EFs, especially in the PG section, upward through the lower Longmaxi Formation (Figs. 7 and 8)records the reestablishment of oxygenated conditions that appear to have continued well into the Rhuddanian Stage.

Algeo and Tribovillard (2009) and Tribovillard et al. (2012) have demonstrated that co-variation patterns of Mo and U enrichment of marine deposits can elucidate bottom water redox conditions, the operation of metal-oxyhydroxide particulate shuttles, and the degree of bottom water restriction that existed during sedimentation. Organic-rich shale deposited under anoxic bottom conditions generally exhibits modest RSTE enrichment and strong RSTE-Mo covariation owing to trace element residence primarily in organic phases (Algeo and Maynard, 2004). However, strong RSTE enrichment and weak RSTE-Mo co-variation documentedfrom carbonaceous shale deposited under euxinic conditions reflects the concentration of trace elements in authigenic sulfide or oxyhydroxide phases (Algeo and Maynard, 2004). Data from both sections displays a good amount of scatter, especially that of the Wufeng Formation (Fig. 11). However, the bulk of the data defines a track extending from a point of roughly equal U and Mo enrichment at low total EFs to one of greater Mo enrichment relative to U at higher total EFs (Fig. 11). Such a trend is suggestive of a change from oxic/suboxic conditions to more intense and/or sustained anoxic, perhaps intermittently euxinic, conditions (Algeo and Tribovillard, 2009; Tribovillard et al., 2012). These data reflect sediment accumulation in what Tribovillard et al. (2012) refer to as an “unrestricted marine” setting in which the supply of Mo to the water column is renewed at a rate that exceededits rate of sequestration in sediment. The preponderance of Mo and U enrichment data fall close to a trend subparallel to a line representing the Mo/U molar ratio of modern seawater

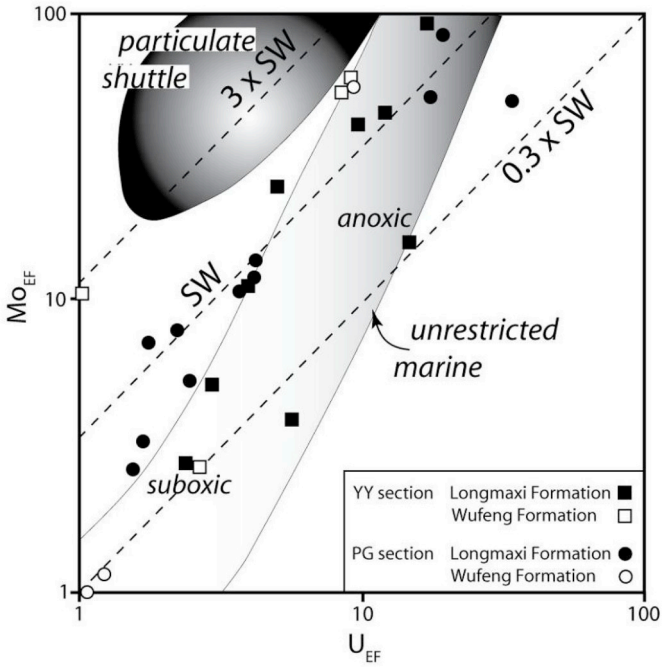

Fig. 11. U_{EF} versus Mo_{EF} scatter plot (log-log) for studied samples of the Wufeng and Longmaxi formations. The unrestricted marine and particulate shuttle fields are from Algeo and Tribovillard (2009) and Tribovillard et al. (2012). Dashed lines define Mo/U molar ratios equal to and greater than seawater (SW and 3 × SW, respectively) and a fraction of seawater (0.3 × SW).Three Wufeng and three Longmaxi samples of the YY section, and four Wufeng and one Longmaxi samples of the PG section plot in a field defined by Mo-EF < 1 and U-EF < 1.

(Mo/U = 1 × SW; Fig. 11). It is noteworthy that there is no evidence (i.e., decreasing Mo enrichment accompanying increasing total enrichment) of an excessive drawdown of aqueous Mo relative to the rate of Mo resupply to the water column – the “basin reservoir effect” (Algeo and Lyons, 2006) – thereby ruling out the existence of a strongly

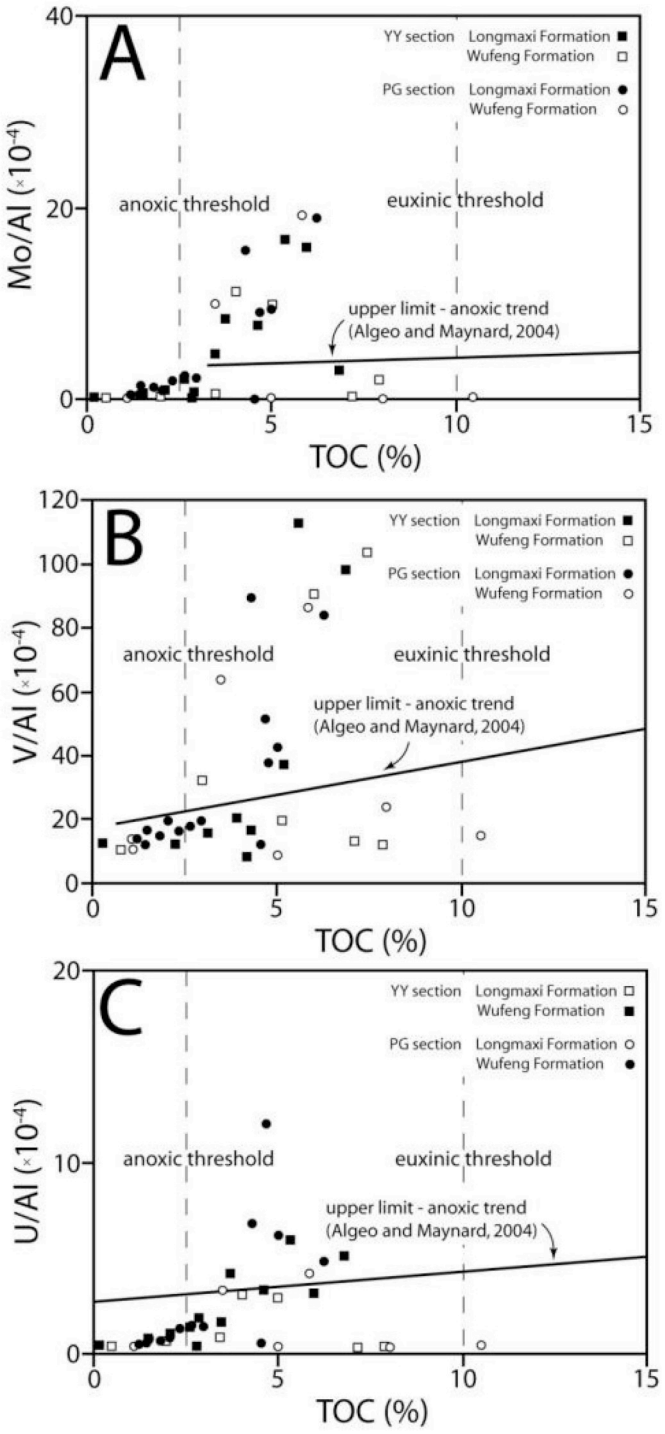

Fig. 12. Cross-plots of (A) Mo, (B) V, and (C) U versus TOC. Various thresholds are from Algeo and Maynard (2004).

restricted basin or a long-standing stable layered water mass during accumulation of the studied deposits. Previous workers have postulated that the Wufeng and Longmaxi formations accumulated in a restricted basin on the upper Yangtze platform (Liu et al., 2017; Zhang et al., 2018). However, Mo—U covariations and Mo/TOC ratios of the present study suggest that the southeastern part of the Yangtze Sea remained connected with the global ocean. Absolute concentrations and EFs of RSTEs as well as their degrees of co-variance with TOC have been used to elucidate redox conditions (Algeo and Maynard, 2004; Algeo and Lyons, 2006; Tribovillard et al., 2009; Scott and Lyons, 2012; Pi et al., 2013). Wufeng and Longmaxi samples analyzed as part of the present study display RSTE-TOC co-variation patterns similar to those described by Algeo and Maynard (2004). Specifically, samples containing less than ~2% TOC define generally flat elemental trends reflecting deposition in association with the detrital fraction under oxic-dysoxic conditions (Fig. 12). Most samples containing > 2% TOC display positive RSTE-TOC co-variance and are distributed below the upper limit-anoxic boundary described by Algeo and Maynard (2004) (Fig. 12). However, a subset of data of each trace element defines a sharp increase of RSTE enrichment at TOC ~2.5–3.0% (Fig. 12). This departure from the anoxic limit is especially obvious in RSTE-TOC plots for Mo and V (Fig. 12A and B). Such sharp increases of trace element enrichment have been described by Algeo and Maynard (2004) at TOC ~ 10%, principally a reflection of a level of oxygen depletion in bottom water that induced the sulfate reduction zone to ascend into the water column. It is noteworthy that TE enrichment among Mo, U, and V based on deviation from the upper limit-anoxic trend appears greatest for V and least for U (Fig. 12). These relationships may reflect the effects of declining benthic dissolved oxygen and/or briefly rising sulfide levels that resulted initially in V enrichment followed by enrichment of Mo as reducing conditions intensified and eventually U accumulation at strongly reducing or even sulfidic conditions. The presence of the two sub-populations likely reflects the effects of alternating anoxic and sulfidic bottom conditions.

4.3. Paleoproductivity

The departure of Si/Al and Ti/Al trends corresponding with the upper Wufeng and lower Longmaxi formations described earlier (Figs. 4 and 5) as well as the presence of radiolaria and sponge spicules in studied samples are consistent with accumulation of these deposits in association with enhanced productivity. Cu and Ni are micronutrients that complex with organic matter under reducing conditions (Piper and Perkins, 2004; Tribovillard et al., 2006). However, the fact these elements display much stronger covariation with Mo, U and V than with bulk accumulation rates of Ba, P, and organic carbon (BaAR, PAR, and OCAR, respectively) (Table 1) suggests that enrichment of Ni and Cu was controlled principally by redox conditions rather than productivity. The lower correlation of BaAR with PAR and OCAR in the PG section ($r = -0.27$ to $+0.11$, $p(\alpha) > 0.05$, $n = 20$; Fig. 6) and modest correlation in the YY section ($r = +0.15$ to $+0.44$, $p(\alpha) > 0.05$, $n = 20$; Fig. 6) may reflect the instability of barite under strongly reducing (sulfate-deficient) diagenetic conditions (Dehairs et al., 1980, 1992; Dymond et al., 1992; Yan et al., 2018). Vertical trends of PAR and OCAR are similar to those of the RSTEs of the Wufeng Formation into the bottom of the Longmaxi Formation (Figs. 7 and 8). Indeed, increasing PAR and OCAR in the middle of the Wufeng Formation in advance of increasing RSTE enrichment, especially in the PG section (Fig. 7), suggests that increasing productivity triggered the establishment of oxygen-depleted conditions. Enhanced marine productivity in association with deposition of the organic-rich upper Wufeng and lower Longmaxi formations and consequent elevated export of organic matter to the sea floor would have diminished or exhausted water column oxygen thereby maintaining or even strengthening anoxic bottom conditions. Primary productivity appears to have diminished during deposition of the upper Longmaxi Formation, especially in the PG section, thus favoring the establishment of more oxygenated conditions during accumulation of these deposits.

4.4. Organicmatter accumulation model

The described trends of clastic sediment content, fluctuating redox conditions, and periods of enhanced paleoproductivity can be synthesized into a depositional model of the Wufeng and Longmaxi formations. Peak sea level on the Yangtze Platform in the early half of the Katian Stage was accompanied by widespread deposition of organic-

Table 1
Correlation coefficients of organic and inorganic geochemical data for the YY (Upper right triangle)and PG sections (Lower left triangle).

	TOC	Al	Ti	ΣREE	L/H	Si	BaAR	PAR	OCAR	Cu-EF	Ni-EF	Mo-EF	V-EF	U-EF
TOC	1	−0.81	−0.76	−0.59	−0.60	−0.47	−0.06	0.38	0.76	0.50	0.67	0.45	0.44	0.46
Al	−0.61	1	0.90	0.76	0.81	0.32	0.30	−0.52	−0.58	−0.41	−0.51	−0.28	−0.24	−0.28
Ti	−0.60	0.98	1	0.93	0.73	0.38	0.30	−0.21	−0.55	−0.43	−0.48	−0.23	−0.17	−0.13
ΣREE	−0.42	0.93	0.92	1	0.63	0.26	0.36	−0.03	−0.38	−0.44	−0.40	−0.25	−0.16	0.00
L/H	−0.25	0.73	0.68	0.66	1	−0.05	0.06	−0.61	−0.57	−0.52	−0.55	−0.37	−0.43	−0.47
Si	−0.59	0.43	0.45	0.42	0.03	1	0.38	0.07	−0.12	0.20	0.18	0.44	0.45	0.35
BaAR	−0.23	0.34	0.42	0.37	0.19	0.56	1	0.15	0.44	0.04	0.33	0.28	0.30	0.41
PAR	0.30	−0.43	−0.38	−0.40	−0.70	−0.10	−0.27	1	0.49	−0.01	0.26	0.14	0.21	0.47
OCAR	0.76	−0.35	−0.32	−0.23	−0.14	−0.17	0.11	0.42	1	0.42	0.74	0.48	0.50	0.55
Cu-EF	−0.01	−0.40	−0.46	−0.30	−0.39	0.33	−0.07	−0.08	−0.03	1	0.65	0.60	0.61	0.40
Ni-EF	0.42	−0.58	−0.60	−0.36	−0.63	0.06	−0.13	0.32	0.27	0.71	1	0.88	0.87	0.82
Mo-EF	0.30	−0.51	−0.51	−0.31	−0.67	0.26	0.07	0.32	0.25	0.69	0.94	1	0.93	0.79
V-EF	0.33	−0.61	−0.61	−0.42	−0.70	0.16	0.01	0.36	0.29	0.70	0.94	0.98	1	0.87
U-EF	0.22	−0.28	−0.31	−0.08	−0.49	0.14	−0.06	0.42	0.21	0.50	0.78	0.71	0.71	1

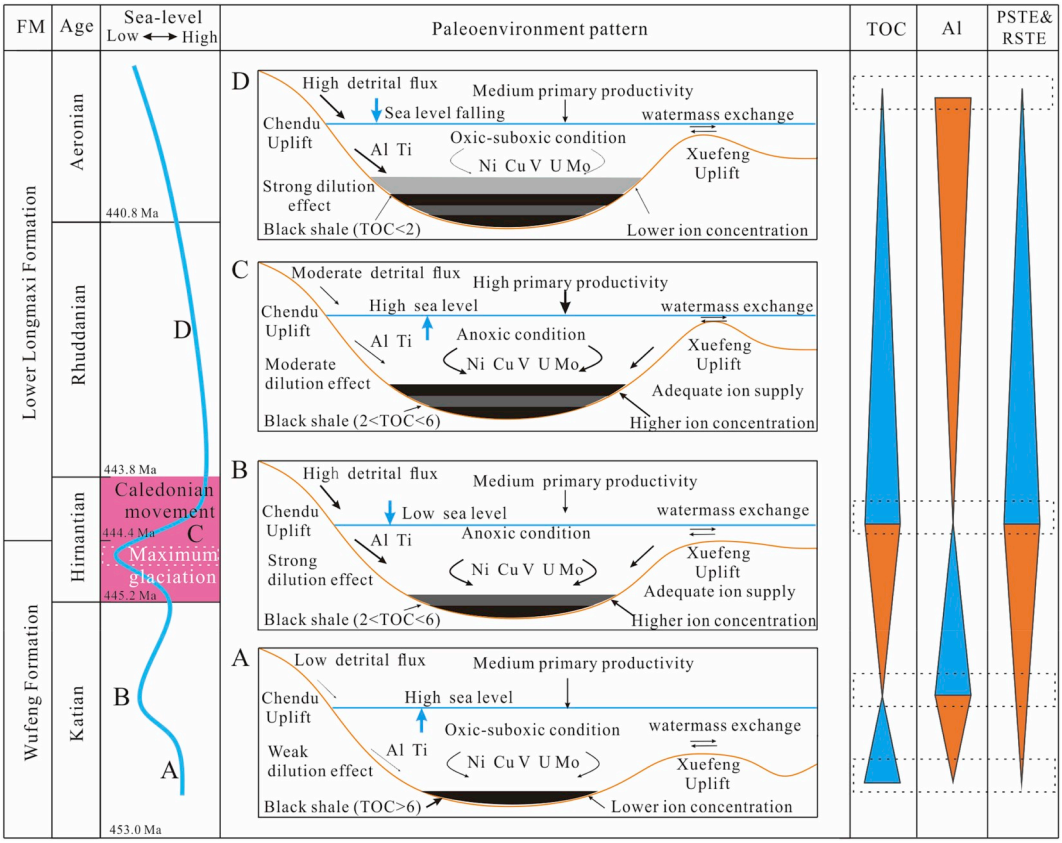

Fig. 13. Organic matter accumulation model of Wufeng and Longmaxi black shales (RSTE and PSTE represent redox-sensitive trace elements and primary productivity -sensitive trace elements, respectively). Sea level curve from (Haq and Schutter, 2008). Refer to text for discussion.

rich siliceous black shale of the lower Wufeng Formation under predominantly suboxic conditions (Xu et al., 2004) (Fig. 13A). Low RSTE, Cu, and Ni enrichment and Si/Al values of these deposits likely reflects unexceptional productivity at this time. Moreover, the negative covariance of Al and TOC (Figs. 4–6) suggests that accumulation of organic matter in the lower Wufeng was favored by a diminshed clastic sediment content (Fig. 13A). A brief regional reduction of sea level and/or tectonic pulse during middle Katian time, perhaps related to uplift of regions bordering the basin, is manifested by an increased abundance of Al and Ti in the middle of the Wufeng Formation and consequent dilution-related reduction of TOC (Fig. 13B).

The beginning of the Hirnantian Stage is marked by aglobal sea level droprelated to the onset of glaciation that was accompanied by deposition of calcareous mudstone of the Kuanyinqiao Bed approximately coincident with the end-Ordovician extinction (Xu et al., 2004). Subsequent melting of glacial ice and consequent rising sea level at the end of the Hirnantian Stage was attended by biotic recovery and expansion (Xu et al., 2004). Rising sea level rise was coincident with increased primary productivity as suggested by Si/Al trends and the presence of radiolarian and sponge spicules. Enhanced productivity and organic matter export to the ocean bottom depleted water column oxygen resulting in the enrichment of RSTEs (Fig. 13C).

The post-glacial global sea level rise was coincident with peak Caledonian tectonic displacement and consequent rapid uplift of regions bordering the Upper Yangtze Platform (Liang et al., 2009; Wang et al., 1997; Xu et al., 2004). However, elevated sea level appears to have maintained the connection of the platform and the global ocean (Fig. 13C) as suggested by Mo-EF and U-EF data (Fig. 11). The

diminished clastic content associated with the post-glacial sea level high stand and elevated productivity favored accumulation of organic-rich deposits of the lower Longmaxi Formation (Fig. 13C). Falling sea level in tandem with peak Caledonian tectonism at the end of the Hirnantian Stage into the Rhuddanian Stage and associated increased clastic content is evidenced by increasing ΣREE, Al, and Ti content upward from the base of the Longmaxi Formation (Xu et al., 2004) (Fig. 13D). Lowering sea level during the Rhuddanian Stage was accompanied by diminished productivity judging from Si/Al trends and the consequent establishment of oxygenated bottom conditions (Yan et al., 2018) (Fig. 13D).

5. Conclusion

The depositional history of organic-rich deposits of the Ordovician-Silurian transition of the economically important Upper Yangtze Basin, South China, reflects the complex interplay of global sea level change, marine productivity, variable clastic content, and regional tectonism. Carbonaceous deposits of the lower Wufeng Formation accumulated under generally suboxic conditions and relatively low clastic sediment content and sedimentation rate during a period of elevated sea level. A brief episode of enhanced clastic sediment content, perhaps the result of incipient Caledonian tectonism, is recorded by deposits of the less carbonaceous middle Wufeng Formation. However, continued rising of sea level and elevated productivity and a diminished clastic content favored accumulation of the organic-rich upper Wufeng Formation and the consequent establishment of oxygen-depleted bottom conditions. The onset of Hirnantian glaciation and related lowered sea level near the end of Wufeng deposition is marked by the calcareous Kuanyinchiao Bed. The subsequent post-glacial sea level rise and increased surface water productivity was attended by accumulation of the carbonaceous lower Longmaxi Formation. Thus, the depositional history of the Ordovician-Silurian transition of the Upper Yangtze Platform reflects the combined effects of regional uplift, variable terrigenous sediment content, and enhanced bioproductivity during a period of fluctuating sea level associated with the expansion and shrinkage of Hirnantian continental glaciation and Caledonian tectonism.

Acknowledgements

We thank Changqing Fu and Zhaobang Cui for assistance with fieldwork. In addition, we would like to thank Professor Algeo for giving us a pertinent revision proposal. This work is supported by the National Science and Technology Major Project (2017ZX05035004-002), the National Postdoctoral Program for Innovative Talents (BX201700282) and the China Postdoctoral Science Foundation (2017M621870).

Appendix A. Supplementary data

Supplementary data to this article can be found online at https://doi.org/10.1016/j.marpetgeo.2019.03.013.

References

Algeo, T.J., Lyons, T.W., 2006. Mo-total organic carbon covariation in modern anoxic marine environments: implications for analysis of paleoredox and paleohydrographic conditions. Paleoceanography 21, PA1016.
Algeo, T.J., Maynard, J.B., 2004. Trace-element behavior and redox facies in core shales of Upper Pennsylvanian Kansas-type cyclothems. Chem. Geol. 206, 289–318.
Algeo, T.J., Rowe, H., 2012. Paleoceanographic applications of trace-metal concentration data. Chem. Geol. 324–325, 6–18.
Algeo, T.J., Tribovillard, N., 2009. Environmental analysis of paleoceanographic systems based on molybdenum–uranium covariation. Chem. Geol. 268, 211–225.
Arthur, M.A., Dean, W.E., 1991. A holistic geochemical approach to cyclomania - examples from Cretaceous pelagic limestone sequences. In: Einsele, G., Ricken, W., Seilacher, A. (Eds.), Cycles and Events in Stratigraphy. Springer-Verlag, Berlin, pp. 126–166.
Arthur, M.A., 1985. Comparative geochemical and mineralogical studies of two cyclic transgressive pelagic limestone units, cretaceous western interior basin, U.S. In: Pratt, L.M., Kauffman, E.G., Zelt, F.B. (Eds.), Fine-grained Deposits and Biofacies of the Western Interior Seaway: Evidence of Cyclic Sedimentary Processes. Society of Economic Paleontologists and Mineralogists, 1985 Midyear Meeting, Golden, Colorado, Field Trip Guidebook No. 4,, pp. 16–27.
Barberi, F., Leoni, L., 2003. Depositional conditions and organic matter preservation pathways in an epicontinental environment: the upper jurassic kashpir oil shales (Volga basin, Russia). Palaeogeogr. Palaeoclimatol. Palaeoecol. 197, 171–197.
Bishop, J.K.B., 1988. The barite-opal-organic carbon association in oceanic particulate matter. Nature 332, 341–343.
Bohacs, K.M., Grabowski Jr., G.J., Carroll, A.R., Mankiewicz, P.J., Miskell-Gerhardt, K.J., Schwalbach, J.R., Wegner, M.B., Simo, J.A., 2005. Production, destruction, and dilution—the many paths to source-rock development. In: Deposition Org.- Carbon-Rich Sediments: Models Mech. Conseq 82. SEPM Special Publications, pp. 61–102.
Boyle, E.A., 1983. Chemical accumulation variations under the Peru Current during the past 130,000 years. J. Geophys. Res 88, 7667–7680.
Brenchley, P.J., Carden, G.A., Hints, L., Kaljo, D., Marshall, J.D., Martma, T., Meidla, T., Nõlvak, J., 2003. High-resolution stable isotope stratigraphy of Upper Ordovician sequences: constraints on the timing of bioevents and environmental changes associated with mass extinction and glaciation. Geol. Soc. Am. Bull. 115, 89–104.
Brenchley, P.J., Marshall, J.D., Carden, G.A.F., Robertson, D.B.R., Long, D.G.F., Meidla, T., Hints, L., Anderson, T.F., 1994. Bathymetric and isotopic evidence for a short-lived late ordovician glaciation in a greenhouse period. Geology 22, 295–298.
Calvert, S.E., Bustin, R.M., Pedersen, T.F., 1992. Lack of evidence for enhanced preservation of sedimentary organic matter in the oxygen minimum of the gulf of California. Geology 20, 757–760.
Calvert, S.E., Pedersen, T.F., 2007. Chapter fourteen elemental proxies for palaeoclimatic and palaeoceanographic Variability in marine sediments: interpretation and application. Dev. Mar. Geol. 1, 567–644.
Chen, J., Xiao, X., 2014. Evolution of nanoporosity in organic-rich shales during thermal maturation. Fuel 129, 173–181.
Chen, X., 1984. Influence of the late ordovician glaciation on basin configuration of the Yangtze platform in China. Lethaia 17, 51–59.
Chen, X., Rong, J.Y., Fan, J., Zhan, R., Mitxhell, C.E., Harper, A.T., Melchin, M.J., Peng, P., Finney, S.C., Wang, X., 2006. The global boundary stratotype section and point (GSSP) for the base of the hirnantian stage (the uppermost of the ordovician System). Episodes 29, 183–196.
Chen, X., Xiao, C.X., Chen, H.Y., 1987. Wufengian (Ashgillian) graptolite faunal differentiation and anoxic environment in south China. Acta Palaeontol. Sin. 15, 1023–1026.
Clarkson, C.R., Solano, N., Bustin, R.M., Bustin, A.M.M., Chalmers, G.R.L., He, L., Melnichenko, Y.B., Radliński, A.P., Blach, T.P., 2013. Pore structure characterization of North American shale gas reservoirs using USANS/SANS, gas adsorption, and mercury intrusion. Fuel 103, 606–616.
Curtis, J.B., 2002. Fractured shale-gas systems. AAPG Bull. 86, 1921–1938.
Dehairs, F., Baeyens, W., Goeyens, L., 1992. Accumulation of suspended barite at mesopelagic depths and export production in the southern ocean. Science 258, 1332–1335.
Dehairs, F., Chesselet, R., Jedwab, J., 1980. Discrete suspended particles of barite and the barium cycle in the open ocean. Earth Planet. Sci. Lett. 49, 528–550.
Demaison, G.J., Moore, G.T., 1980. Anoxic environments and oil source bed genesis. Org. Geochem. 2, 9–31.
Deng, J.X., Tang, Z.Y., Li, Y., 2018. The influence of the diagenetic process on seismic rockphysical properties of Wufeng and Longmaxi Formation shale. Chinese J. Geophys. 61, 659–672.
Dong, D., Gao, S., Huang, J., Guan, Q., Wang, S., Wang, Y., 2015. Discussion on the exploration & development prospect of shale gas in the Sichuan Basin. Nat. Gas. Ind. 2, 9–23.
Dymond, J., Suess, E., Lyle, M., 1992. Barium in deep-sea sediment: a geochemical proxy for paleoproductivity. Paleoceanography 7, 163–181.
Dypvik, H., Harris, N.B., 2001. Geochemical facies analysis of fine-grained siliciclastics using Th/U, Zr/Rb and (Zr + Rb)/Sr ratios. Chem. Geol. 181, 131–146.
Franchi, F., Turetta, C., Cavalazzi, B., Corami, F., Barbieri, R., 2016. Trace elements and REE geochemistry of middle devonian carbonate mounds (maïder basin, eastern anti-atlas, Morocco): implications for early diagenetic processes. Sediment. Geol. 343, 56–71.
Gromet, L.P., Haskin, L.A., Korotev, R.L., Dymek, R.F., 1984. The “North American shale composite”: its compilation, major and trace element characteristics. Geochem. Cosmochim. Acta 48, 2469–2482.
Haq, B.U., Schutter, S.R., 2008. A chronology of paleozoic sea-level changes. Science 322, 64–68.
Haskin, L.A., Frey, F.A., Schmitt, R.A., Smith, R.H., 1966. Meteoritic, solar and terrestrial rare-earth distributions. Phys. Chem. Earth 7, 167–321.
He, J.L., Liu, W., Yang, P., Qian, Y.U., Wang, J., Wang, Z.J., Jun-Ze, L.U., Qin, C., Center, C., 2017. Genetic conditions of the shale gas and delineation of the favourable areas in the Wufeng Formation-Longmaxi Formation on the southwestern margin of the Sichuan Basin. Sediment. Geol. Tethyan Geol. 37, 50–58.
Huang, H., He, D., Li, Y., Li, J., Zhang, L., 2017. Silurian tectonic-sedimentary setting and basin evolution in the Sichuan area, southwest China: implications for palaeogeographic reconstructions. Mar. Petrol. Geol. 92, 403–423.
Ibach, L.E., 1980. Relationship between sedimentation rate and total organic carbon content in ancient marine sediments. Am. Assoc. Pet. Geol. 66, 170–188.
Jarvie, D.M., Hill, R.J., Ruble, T.E., Pollastro, R.M., 2007. Unconventional shale-gas systems: the Mississippian Barnett Shale of north-central Texas as one model for thermogenic shale-gas assessment. AAPG Bull. 91, 475–499.
Jiang, S.Y., Zhao, H.X., Chen, Y.Q., Yang, T., Yang, J.H., Ling, H.F., 2007. Trace and rare earth element geochemistry of phosphate nodules from the lower Cambrian black shale sequence in the Mufu Mountain of Nanjing, Jiangsu province, China. Chem. Geol. 244, 584–604.
Lash, G.G., Blood, D.R., 2014. Organic matter accumulation, redox, and diagenetic history

of the Marcellus Formation, southwestern Pennsylvania, Appalachian basin. Mar. Petrol. Geol. 57, 244–263.
Lev, S.M., Mclennan, S.M., Meyers, W.J., Hanson, G.N., 1998. A petrographic approach for evaluating trace-element mobility in a black shale. J. Sediment. Res. 68, 970–980.
Li, S.J., Xiao, K.H., Wo, Y.J., Long, S.X., Cai, L.G., 2008. Developmental controlling factors of upper ordovician-lower silurian high quality source rocks in marine sequence, south China. Acta Sedimentol. Sin. 5, 872–880.
Li, Y., Zhang, T., Ellis, G.S., Shao, D., 2017. Depositional environment and organic matter accumulation of upper ordovician–lower silurian marine shale in the upper Yangtze platform, south China. Palaeogeogr. Palaeoclimatol. Palaeoecol. 466, 252–264.
Liang, D., Guo, T., Chen, J., Bian, L., Zhao, Z., 2009. Some progresses on studies of hydrocarbon generation and accumulation in marine sedimentary regions, southern China (Part 2):Geochemical characteristics of four suits of regional marine source rocks, south China. Mar. Origin Petrol. Geol. 14, 1–15.
Liu, Z., Algeo, T.J., Guo, X., Fan, J., Du, X., Lu, Y., 2017. Paleo-environmental cyclicity in the early silurian Yangtze Sea (south China): tectonic or glacio-eustatic control? Palaeogeogr. Palaeoclimatol. Palaeoecol. 466, 59–76.
Ma, Y., Fan, M., Lu, Y., Guo, X., Hu, H., Chen, L., Wang, C., Liu, X., 2016. Geochemistry and sedimentology of the Lower Silurian Longmaxi mudstone in southwestern China: implications for depositional controls on organic matter accumulation. Mar. Petrol. Geol. 75, 291–309.
McLennan, S.M., 2001. Relationships between the trace element composition of sedimentary rocks and upper continental crust. Geochem. Geophys. Geosyst. 2 (2000GC00109), 24.
Metcalfe, I., 1994. Late palaeozoic and mesozoic palaeogeography of eastern pangea and tethys. Can. Soc. Pet. Geol., Mem. 17, 97–111.
Murray, R.W., 1994. Chemical criteria to identify the depositional environment of chert: general principles and applications. Sediment. Geol. 90, 213–232.
Norman, M.D., Deckker, P.D., 1990. Trace metals in lacustrine and marine sediments: a case study from the Gulf of Carpentaria, northern Australia. Chem. Geol. 82, 299–318.
Passey, Q.R., Bohacs, K., Esch, W.L., Klimentidis, R., Sinha, S., 2010. From oil-prone source rock to gas-producing shale reservoir - geologic and petrophysical characterization of unconventional shale gas reservoirs. In: International Oil and Gas Conference and Exhibition in China, 8-10 June. Society of Petroleum Engineers, SPE, Beijing, China, pp. 131350.
Paytan, A., Moore, W.S., Kastner, M., 1996. Sedimentation rate as determined by 226Ra activity in marine barite. Geochem. Cosmochim. Acta 60, 4313–4319.
Pedersen, T.F., 1990. Anoxia vs. productivity : what controls the formation of organic carbon rich sediments and sedimentary rocks? Am. Assoc. Petrol. Geol. Bull. 74, 454–466.
Pi, D.H., Liu, C.Q., Shields-Zhou, G.A., Jiang, S.Y., 2013. Trace and rare earth element geochemistry of black shale and kerogen in the early Cambrian Niutitang Formation in Guizhou province, South China: constraints for redox environments and origin of metal enrichments. Precambrian Res. 225, 218–229.
Piper, D.Z., Perkins, R.B., 2004. A modern vs. Permian black shale—the hydrography, primary productivity, and water-column chemistry of deposition. Chem. Geol. 206, 177–197.
Rimmer, S.M., 2004. Geochemical paleoredox indicators in devonian–mississippian black shales, central appalachian basin (USA). Chem. Geol. 206, 373–391.
Rimmer, S.M., Thompson, J.A., Goodnight, S.A., Robl, T.L., 2004. Multiple controls on the preservation of organic matter in Devonian–Mississippian marine black shales: geochemical and petrographic evidence. Palaeogeogr. Palaeoclimatol. Palaeoecol. 215, 125–154.
Sageman, B.B., Lyons, T.W., 2004. Geochemistry of fine-grained sediments and sedimentary rocks. Treatise Geochem 7, 115–158.
Sageman, B.B., Murphy, A.E., Werne, J.P., Straeten, C.A.V., Hollander, D.J., Lyons, T.W., 2003. A tale of shales: the relative roles of production, decomposition, and dilution in the accumulation of organic-rich strata, Middle–Upper Devonian, Appalachian basin. Chem. Geol. 195, 229–273.
Sanchez-Vidal, A., Collier, R.W., Calafat, A., Fabres, J., Canals, M., 2005. Particulate barium fluxes on the continental margin: a study from the Alboran Sea (western Mediterranean). Mar. Chem. 93, 105–117.
Schmitz, B., 1987. Barium, equatorial high productivity, and the northward wandering of the Indian continent. Paleoceanography 2, 63–77.
Schneider, R.R., Price, B., Müller, P.J., Kroon, D., Alexander, I., 1997. Monsoon related variations in Zaire (Congo) sediment load and influence of fluvial silicate supply on marine productivity in the east equatorial Atlantic during the last 200,000 years. Paleoceanography 12, 463–481.
Schoepfer, S.D., Shen, J., Wei, H.Y., Tyson, R.V., Ingall, E., Algeo, T.J., 2015. Total organic carbon, organic phosphorus, and biogenic barium fluxes as proxies for paleomarine productivity. Earth Sci. Rev. 149, 23–52.
Schütz, L., Rahn, K.A., 1982. Trace-element concentrations in erodible soils. Atmos. Environ. 16, 171–176.
Scott, C., Lyons, T.W., 2012. Contrasting molybdenum cycling and isotopic properties ineuxinic versus non-euxinic sediments and sedimentary rocks: refining the paleoproxies. Chem. Geol. 324, 19–27.
Shimmield, G.B., Mowbray, S.T., 1991. The inorganic geochemical record of the northwest Arabian Sea: a history of productivity variation over the last 400 K.Y. from sites 722 and 724. Proc. Ocean Drill. Progr. Sci. Results 117, 409–419.
Tan, J., Horsfield, B., Fink, R., Kroos, B., Schulz, H.-M., Rybacki, E., Zhang, J., Borcham, C.J., van Grass, G., Tocher, B.A., 2014. Shale gas potential of the major marine shale formations in the Upper Yangtze Platform, South China, Part III. Mineralogical, lithological, petrophysical, and rock mechanical properties. Energy Fuels 28, 2322–2342.
Tribovillard, N., Algeo, T.J., Baudin, F., Riboulleau, A., 2012. Analysis of marine environmental conditions based on molybdenum–uranium covariation—applications to Mesozoic paleoceanography. Chem. Geol. 324–325, 46–58.
Tribovillard, N., Algeo, T.J., Lyons, T., Riboulleau, A., 2006. Trace metals as paleoredox and paleoproductivity proxies: an update. Chem. Geol. 232, 12–32.
Tribovillard, N., Bout-Roumazeilles, V., Sionneau, T., Montero-Serrano, J.C., Riboulleau, A., Baudin, F., 2009. Does a strong pycnocline impact organic-matter preservation and accumulation in an anoxic setting? The case of the Orca Basin, Gulf of Mexico. Cr. Geosci 341, 1–9.
Vandenbroucke, M., Largeau, C., 2007. Kerogen origin, evolution and structure. Org. Geoshem. 38, 719–833.
VerStraeten, C.A., Brett, C.E., Sageman, B.B., 2011. Mudrock sequence stratigraphy: a multi-proxy (sedimentological, paleobiological and geochemical) approach, Devonian Appalachian Basin. Palaeogeogr. Palaeoclimatol. Palaeoecol. 304, 21–53.
Wang, C., Zhang, B., Lu, Y., Shu a, Z., Lu, Y., Bao, Ha, Meng, Z., Chen, L., 2018. Lithofacies distribution characteristics and its controlling factors of shale in Wufeng Formation-Member 1 of Longmaxi Formation in the Jiaoshiba area. Petrol. Res. 4, 306–319.
Wang, K., Chatterton, B.D.E., Wang, Y., 1997. An organic carbon isotope record of Late Ordovician to Early Silurian marine sedimentary rocks, Yangtze Sea, South China: implications for CO2 changes during the Hirnantian glaciation. Palaeogeogr. Palaeoclimatol. Palaeoecol. 132, 147–158.
Wang, X., Zhu, Y., Fu, C., 2019. Experimental investigation of the stress-dependent permeability in the Longmaxi Formation shale. J. Pet. Sci. Eng. 175, 932–947.
Wang, Y., Chen, B., Li, X., 2018. Sedimentary characteristics of ascending oceanic shale in the lower silurian Longmaxi formation in the northeastern sichuan basin. Acta. Petrol. Ei. Sinica 39, 1094–1104.
Wang, Y., Xua, S., Hao, F., Lua, Y., Shu, Z., Yana, D., Lua, Y., 2019. Geochemical and petrographic characteristics of Wufeng-Longmaxi shales, Jiaoshiba area, southwest China: implications for organic matter differential accumulation. Mar. Petrol. Geol. 102, 138–154.
Wang, Y., Zhu, Y., Liu, S., Zhang, R., 2016. Pore characterization and its impact on methane adsorption capacity for organic-rich marine shales. Fuel 181, 227–237.
Wedepohl, K.H., 1971. Environmental influences on the chemical composition of shales and clays. In: Ahrens, L.H., Press, F., Runcorn, S.K., Urey, H.C. (Eds.), Phys. Chem. Earth. Pergamon, Oxford, pp. 305–333.
Wedepohl, K.H., 1991. The composition of the upper earth's crust and the natural cycles of selected metals.Metals in natural raw materials. Natural Resources. In: Merian, E. (Ed.), Metals and Their Compounds in the Environment. VCH, Weinheim, pp. 3–17.
Werne, J.P., Lyons, T.W., Hollander, D.J., Formolo, M.J., Damsté, J.S.S., 2003. Reduced sulfur in euxinic sediments of the Cariaco Basin: sulfur isotope constraints on organic sulfur formation. Chem. Geol. 195, 159–179.
Xu, C., Jiayu, R., Mitchell, C.E., Harper, D.A.T., Junxuan, F., Renbin, Z., Yuandong, Z., Yu, L.R., Yi, W., 2000. Late Ordovician to earliest Silurian graptolite and brachiopod biozonation from the Yangtze region, South China, with a global correlation. Geol. Mag. 137, 623–650.
Xu, C., Rong, J.Y., Yue, L., Boucot, A.J., 2004. Facies patterns and geography of the Yangtze region, South China, through the ordovician and silurian transition. Palaeogeogr. Palaeoclimatol. Palaeoecol. 204, 353–372.
Yan, C., Jin, Z., Zhao, J., Du, W., Liu, Q., 2018. Influence of sedimentary environment on organic matter enrichment in shale: a case study of the Wufeng and Longmaxi Formations of the Sichuan Basin, China. Mar. Petrol. Geol. 92, 808–894.
Yan, D., Wang, H., Fu, Q., Chen, Z., He, J., Gao, Z., 2015. Geochemical characteristics in the Longmaxi formation (early silurian) of South China: implications for organic matter accumulation. Mar. Petrol. Geol. 65, 290–301.
Yang, B., Kang, Y., You, L., Li, X., Chen, Q., 2016a. Measurement of the surface diffusion coefficient for adsorbed gas in the fine mesopores and micropores of shale organic matter. Fuel 181, 793–804.
Yang, R., He, S., Hu, Q., Hu, D., Yi, J., 2017. Geochemical characteristics and origin of natural gas from Wufeng-Longmaxi shales of the Fuling gas field, Sichuan Basin (China). Int. J. Coal Geol. 171, 1–11.
Yang, Z., Wang, W., Dong, M., Wang, J., Li, Y., Gong, H., Sang, Q., 2016b. A model of dynamic adsorption–diffusion for modeling gas transport and storage in shale. Fuel 173, 115–128.
Yu, W., Jie, P., Wang, L., Wang, J., Zheng, J., Song, Y.F., Wang, C.C., Wang, Y., Chan, J., 2016. Characterization of typical 3D pore networks of Jiulaodong formation shale using nano-transmission X-ray microscopy. Fuel 170, 84–91.
Zabel, M., Bickert, T., Dittert, L., Haese, R.R., 1999. Significance of the sedimentary Al:Ti ratio as an indicator for variations in the circulation patterns of the equatorial North Atlantic. Paleoceanography 14, 789–799.
Zabel, M., Schneider, R.R., Wagner, T., Adegbie, A.T., deVries, U., Kolonic, S., 2001. Late Quaternary climate changes in central Africa as inferred from terrigenous input to the Niger Fan. Quat. Res. (Tokyo) 56, 207–217.
Zhang, K., Song, Y., Jiang, S., Jiang, Z., Jia, C., Huang, Y., Wen, M., Liu, W., Xie, X., Liu, T., Wang, P., Shan, C., Wu, Y., 2018. Mechanism analysis of organic matter enrichment in different sedimentary backgrounds: a case study of the Lower Cambrian and the Upper Ordovician-Lower Silurian, in Yangtze region. Mar. Petrol. Geol. 99, 488–497.
Zhang, M., Yao, J., Sun, H., Zhao, J.L., Fan, D.Y., Huang, Z.Q., Wang, Y.Y., 2015. Triple-continuum modeling of shale gas reservoirs considering the effect of kerogen. J. Nat. Gas Sci. Eng. 24, 252–263.
Zhou, L., Algeo, T.J., Shen, J., Hu, Z.F., Gong, H., Xie, S., Huang, J.H., Gao, S., 2015. Changes in marine productivity and redox conditions during the Late Ordovician Hirnantian glaciation. Palaeogeogr. Palaeoclimatol. Palaeoecol. 420, 223–234.